Metal–Organic Frameworks

International Edition: DOI: 10.1002/anie.201510855
German Edition: DOI: 10.1002/ange.201510855

Proton Transport in a Highly Conductive Porous Zirconium-Based Metal–Organic Framework: Molecular Insight

Daiane Damasceno Borges, Sabine Devautour-Vinot, Hervé Jobic,* Jacques Ollivier, Farid Nouar, Rocio Semino, Thomas Devic, Christian Serre, Francesco Paesani,* and Guillaume Maurin*

Abstract: *The water stable UiO-66(Zr)-$(CO_2H)_2$ MOF exhibits a superprotonic conductivity of 2.3×10^{-3} S cm^{-1} at 90 °C and 95 % relative humidity. Quasi-elastic neutron scattering measurements combined with aMS-EVB3 molecular dynamics simulations were able to probe individually the dynamics of both confined protons and water molecules and to further reveal that the proton transport is assisted by the formation of a hydrogen-bonded water network that spans from the tetrahedral to the octahedral cages of this MOF. This is the first joint experimental/modeling study that unambiguously elucidates the proton-conduction mechanism at the molecular level in a highly conductive MOF.*

There is a growing interest in the discovery of novel proton-conducting solids for further applications as proton-exchange membranes, key components in diverse energy-related technologies, including fuel cells, water electrolysers and redox flow batteries.[1] Recently, porous crystalline hybrid solids, metal organic frameworks (MOFs), have shown promising performances for both water-mediated and water-free (i.e. anhydrous or with the incorporation of protonic organic guests) proton conduction operating at $T<100$ °C and $T\geq 100$ °C respectively.[2–6] Inspired by the advances made in the field of solid-state proton conductors, the best MOFs were mostly devised in such a way to contain on one hand a high concentration of proton sources created by either the decoration of the pore walls with acidic groups (sulfonic[7] or phosphonic[8]) or the presence of counterions or acidic molecules into the pores[9,10] and to favor on the other hand the formation of an hydrogen-bonded network as conduction pathway for an efficient proton transport through the incorporation of water or protonic guest molecules like imidazole, triazole or histamine.[11] This led to a handful of MOFs materials that largely compete with the performances of Nafion under humidification.[2–6,12,13] While this effort of materials design has been relatively successful so far, a better understanding of the proton transport mechanism could pave the way towards optimized MOFs by fine-tuning the key features of their architectures. Up to date, the mechanisms related to the mobility of protons in these hybrid solids have been identified basically from the values of the activation energy obtained by complex impedance spectroscopy (CIS).[2–6,12,13] Two general mechanisms for water-mediated proton transport in MOFs, commonly referred to Grotthuss and vehicular mechanisms,[14,15] have been proposed although they are generally poorly supported by a microscopic description of the proton and/or water dynamics. To the best of our knowledge, except for the theoretical work previously published by one of us on the model MIL-53(Cr) solid,[16] it is the first time that a joint experimental/computational study explores at the molecular level the mobility of the charge carriers in MOFs. A combination of quasi-elastic neutron scattering (QENS) measurements and molecular dynamics (MD) simulations was applied to a hydrolytic microporous robust and highly hydrophilic functionalized microporous Zr-based MOF, that is, UiO-66(Zr)-$(CO_2H)_2$ or $Zr_6O_4(OH)_4(O_2C\text{-}C_6H_2\text{-}CO_2\text{-}(CO_2H)_2)_6\cdot x\,H_2O$ ($x\approx16$), UiO standing for University of Oslo.[17] The strongly confined environment of this functionalized MOF, that bears a high concentration of free CO_2H groups together with the presence of small and bulky microporous cages connected by narrow triangular windows makes the fundamental understanding of the transport mechanism challenging. From a practical application standpoint, above the attractive features of this solid in terms of soft and green synthesis conditions and high chemical robustness,[17] preliminary investigations suggested that UiO-66(Zr)-$(CO_2H)_2$ might be a promising candidate for proton conductivity (see the Supporting Information).[18]

CIS measurements performed as a function of the temperature at 95 % relative humidity (RH; see Figure S4 and details of the data analysis are given in the Experimental

[*] Dr. D. D. Borges, Dr. S. Devautour-Vinot, Dr. R. Semino, Prof. G. Maurin
Institut Charles Gerhardt Montpellier UMR 5253 CNRS UM ENSCM
Université Montpellier
Pl. E. Bataillon, 34095 Montpellier cedex 05 (France)
E-mail: sabine.devautour-vinot@um2.fr
Dr. H. Jobic
Institut de Recherches sur la Catalyse et l'Environnement de Lyon CNRS, Université de Lyon
2. Av. A. Einstein, 69626, Villeurbanne (France)
E-mail: herve.jobic@ircelyon.univ-lyon1.fr
Dr. J. Ollivier
Institut Laue Langevin
BP 156, 38042 Grenoble (France)
Dr. F. Nouar, Dr. T. Devic, Dr. C. Serre
Institut Lavoisier Versailles, UMR 8180 CNRS
Université de Versailles
45 Av. des Etats-Unis, 78035 Versailles, cedex (France)
Prof. F. Paesani
Department of Chemistry and Biochemistry
University of California, San Diego
La Jolla, CA 92093 (USA)
E-mail: fpaesani@ucsd.edu
Supporting information and the ORCID identification number(s) for the author(s) of this article can be found under http://dx.doi.org/10.1002/anie.201510855.

Section) indicate that the conductivity (σ) of UiO-66(Zr)-$(CO_2H)_2$ increases from 8.5×10^{-4} S cm^{-1} (25 °C) to 2.3×10^{-3} S cm^{-1} (90 °C) (Figure 1), illustrating the superprotonic behavior of this MOF ($\sigma > 10^{-4}$ S cm^{-1}).[19]

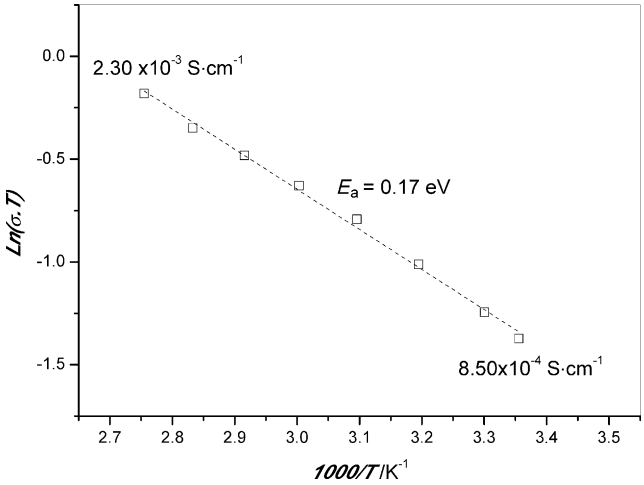

Figure 1. Plot of the logarithm of the proton conductivity at 95% RH as a function of the inverse temperature for UiO-66(Zr)-$(CO_2H)_2$. The dashed line corresponds to the Arrhenius fit.

The value of σ measured at 90 °C is comparable with those collected under humid conditions for the best water-mediated proton-conducting MOFs reported so far.[2,–6,12,13] Interestingly, the performances of this solid are maintained after consecutive heating and cooling cycles (see Figure S5). Moreover, the activation energy deduced from the Arrhenius plot (see Figure 1, $E_a = 0.17$ eV), is among the lowest values reported for other hybrid porous solids[2–6] which suggests a highly efficient water-mediated proton transport. This value falls into the [0.1–0.4 eV] range which is usually related to a Grotthuss-like mechanism.[15]

In order to shed light onto the water-mediated proton transport in UiO-66(Zr)-$(CO_2H)_2$, QENS experiments were also carried out. This technique is particularly suited to follow the diffusion of hydrogen, or hydrogen-containing molecules, because of the large cross-section of hydrogen.[20] Furthermore, since this cross-section is incoherent, one can probe individual proton dynamics. QENS has been used in the past to characterize the diffusion of dihydrogen in porous solids like zeolites and MOFs and of hydrogen in metal hydrides.[21–23] Proton motion has been less studied.[24–30] Diffusion coefficients have been obtained in proton-conducting oxides,[24] but local and long-range motions must be disentangled, and there are complications due to trapping or disorder. Attempts were made to investigate acidic aqueous solutions,[25] however the proton motion is coupled to diffusive motions of the vehicles (H_2O or H_3O^+). Confinement plays a big role in perfluorinated sulfonic membranes, where localized translational motions, fast rotational motions and slow hopping of protons in the vicinity of the sulfonic charges have been reported.[26] Acidic clathrate hydrates are easier to study than solutions or liquids because the translational degrees of freedom of water are substantially reduced.[27–29]

Here, the QENS measurements were performed on a fully hydrated UiO-66(Zr)-$(CO_2H)_2$ sample in the temperature range of 300–373 K. Two QENS spectra obtained at relatively low and high Q are reported in Figure 2. The spectra were first

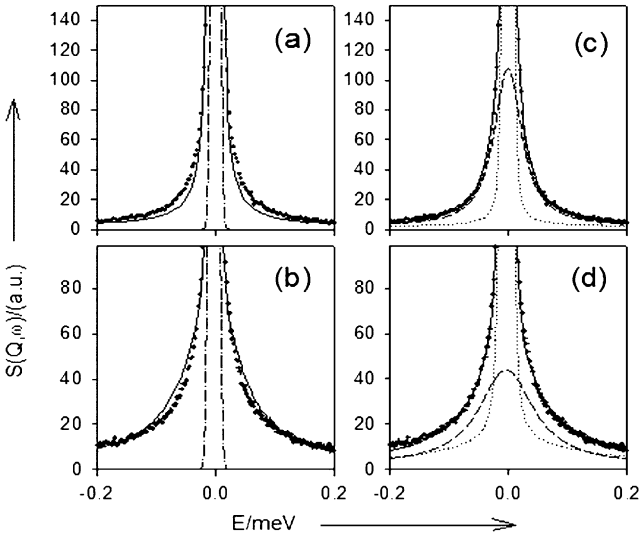

Figure 2. Comparison between experimental (+) and calculated QENS spectra obtained at 373 K for the fully hydrated UiO-66(Zr)-$(CO_2H)_2$, at (a,c) $Q = 0.26$ Å^{-1}, and (b,d) $Q = 0.96$ Å^{-1}. The solid lines correspond to (a,b) one proton diffusing and rotating, and (c,d) a proton (dashed line) plus a water molecule (dotted line). The instrumental resolution, of Gaussian shape, is indicated by the dotted-dashed lines in (a) and (b).

fitted with the model appropriate to the acidic clathrate hydrates: all protons are dynamically equivalent and located within "clouds" surrounding the oxygen atoms (hydronium and water species).[27–29] Proton diffusion results from jumps between the protonic clouds, which are only performing local reorientational motions, that is, no diffusion of oxygen atoms is observed. Fits with this model lead to broadenings which are too narrow at low Q and too large at high Q, as shown in Figure 2a and 2b, even using various models for the localized motions: rotation inside or on the surface of a sphere, or uniaxial rotation. The only possibility to fit satisfactorily the spectra was to consider that two dynamical species are observed on the time scale of the experiment: a "free" proton performing long-range diffusion and a diffusing and rotating water molecule, with a ratio proton/water varying with temperature in the range 300–373 K. Refinements with this model led to an improvement to the fit, with weighted profile R factors, R_{wp}, decreasing from 12.2% to 7.7%, for the 9 spectra measured at 373 K in the selected Q range. Refinements show that the proton diffuses faster than water (the reverse yielding poorer fits). The self-diffusion coefficients, D_s, were obtained by fitting the spectra measured at small Q with a Fickian diffusion model, the estimated error varying between 50% at 373 K and a factor 2 at 300 K, because the broadenings get smaller when the temperature is reduced.

Proton diffusion is characterized by a D_s of 3.5×10^{-9} $m^2 s^{-1}$, at 373 K, with an activation energy of 0.15 eV (Figure 3) in good agreement with the value obtained by CIS measurements. Water diffuses about one order of magnitude slower, with a D_s of 1.4×10^{-10} $m^2 s^{-1}$, at 373 K, and a larger activation energy, that is, 0.20 eV. Both dynamics are slower than those reported for the bulk water ($D_s(H_2O) = 2.3 \times 10^{-9}$ $m^2 s^{-1}$ and $D_s(H^+) = 9.4 \times 10^{-9}$ $m^2 s^{-1}$ at 300 K).[31,32] The rotational motion of water was described by a rotational diffusion model, with a correlation time τ of 57 ps at 300 K, and an activation energy of 0.14 eV.

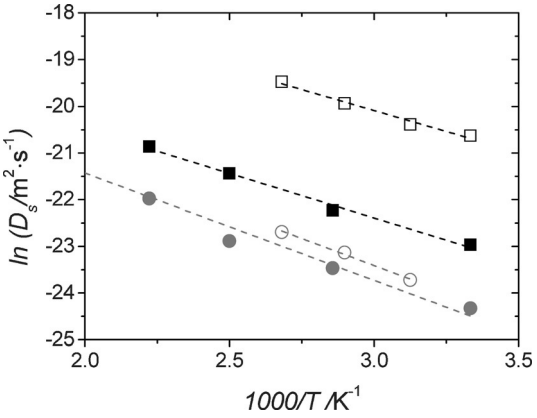

Figure 3. Arrhenius plot of D_s for protons (squares) and water molecules (circles) in the fully hydrated UiO-66(Zr)-$(CO_2H)_2$: QENS (open symbols) and aMS-EVB3-MD simulations (full symbols).

similar to the experimental value (0.17 eV vs. 0.15 eV) and remains lower as compared to that for water (0.20 eV).

The proton-hopping event between H_2O molecules can be conveniently identified by tracking the conversion of the CEC at the vicinity of an *i*th oxygen atom ("pivot hydronium") to a *j*th oxygen atom (new "pivot hydronium") through the MOF pores along the MD runs.[16,33] The time decay of the pseudo-continuous correlation function Cpc(t) is defined as $\mathrm{Cpc}(t) = \langle h_i(0)h_i(t)\rangle / \langle h_i(0)h_i(0)\rangle$ where $h_i(t) = 1$ if the *i*th oxygen atom is the pivot hydronium oxygen, and zero otherwise.[16,33,34,37] Figure 4 shows that Cpc(t) slowly decays

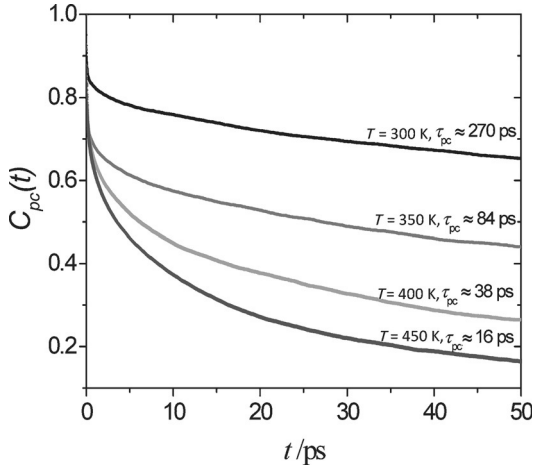

Figure 4. Pseudo-continuous time correlation function calculated from the aMS-EVB3-MD simulations at different temperatures.

Molecular dynamics simulations, using the anharmonic multistate empirical valence bond (aMS-EVB3) model,[33,34] were performed in the NVE ensemble at temperatures ranging from 300 K to 450 K to provide a detailed molecular-level picture of the transport mechanism in play. This computational approach which has been successfully employed in the past to model proton transport in aqueous environments,[35,36] allows the mobility of both an excess proton and the water molecules to be simultaneously followed. Here UiO-66(Zr)-$(CO_2H)_2$ was investigated as fully hydrated and treated using our previously derived flexible force field (see details in the Experimental Section).[17] From the mean-square displacement (MSD) curves averaged over multiple time origins and five different MD trajectories, it was thus possible to extract the self-diffusion coefficient D_s for both water and the center of excess charge (CEC) using the Einstein relation. The simulated D_s for H_2O and the associated activation energy ($E_a = 0.20$ eV) are in excellent agreement with the QENS data (Figure 3). These calculations further confirmed that the self-diffusivity of the proton is faster as compared to water although the simulated D_s(CEC) underestimates the corresponding QENS value. This observation supports that the transport of the excess proton is largely governed by the Grotthuss mechanism rather than a vehicular scenario where the excess proton would be transported along with the water molecules that solvate it.[15] The simulated activation energy for the proton diffusion is at room temperature. The relaxation time, τ_{PC} obtained from the fits to the long-time decay of $C_{pc}(t)$ at 300 K of approximately 270 ps is significantly longer than the corresponding value for an excess proton in bulk water (ca. 1.7 ps).[38] This observation emphasizes that the water-mediated proton dynamics in the MOF is largely restricted to local displacements at ambient temperature corresponding to intra-cages motions. Figure 4 further shows that when the temperature increases, τ_{PC} significantly drops and hence the proton diffusivity becomes faster (Figure 3). This suggests a significant rearrangement of the water molecules at high temperature in such a way to ensure a more efficient proton transfer through the entire porosity of UiO-66(Zr)-$(CO_2H)_2$.

A careful inspection of the MD trajectories evidenced that the water molecules are mostly distributed in the tetrahedral cages at 300 K (Figure S14) forming relatively strong interactions with the free CO_2H functions grafted on the linker (see the corresponding radial distribution functions in Figure S9). This in turn drastically reduces not only the translational dynamics of the confined H_2O (Figure 3) but also their rotational motions as illustrated by the slow simulated rotational correlation time of 22 ps within the same range of the value than the QENS findings. These water molecules preferentially form clusters assembling up to 10 molecules with the formation of a 3D-bonded arrangement in the available space of the cages. Further, the radial distribution function between O(H_2O)-O(H_3O^+) shows a first peak

centered around 2.5 Å which integrates to 3.0 at its first minimum (see Figure S10). These findings are in line with Eigen's view corresponding to the formation of a hydrated hydronium ion ($H_9O_4^+$).[39] At this temperature, the water molecules are characterized by long residence times (ca. 3 ns) in the tetrahedral cages and only a few of them travel over long distances from the tetrahedral to the octahedral cages by crossing the narrow triangular windows. This hampers the formation of a percolated hydrogen-bond network through the pores and hence implies that the excess charge only rarely migrates from one cage to another.

At higher temperature, the water molecules are equally distributed in both the tetrahedral and octahedral cages, which is consistent with a significant decrease of the residence times in the tetrahedral cages by a factor of 20 (ca. 125 ps; Figure S14). Interestingly an H-bond network that bridges the two cages can be formed. The analysis of the hydrogen-bonded (HB) network size distribution (see the Supporting Information) shows that H_2O preferentially form much longer HB networks as compared to the situation at ambient temperature, with more than 60% of the total water molecules being part of this network (see Figure S12). Moreover, the average number of H-bonds per water molecules is significantly lower than in the bulk water (3.6)[40] and globally decreases from 2.4 (300 K) to 2.0 (450 K). This trend suggests a reorganization of the confined water molecules at high temperature that favors the formation of a percolating HB network. Furthermore, the HB lifetime is much shorter (18 ps vs. 1000 ps at 450 K and 300 K, respectively, Figure S13) which is consistent with a much less packed geometry for H_2O within the pores (Figure S14) and a faster rotational correlation time (0.8 ps). All together the spatial arrangement and the dynamics of H_2O offer an optimal scenario to allow a proton shuttling over long distances. This is illustrated in Figure 5 which reports the positions occupied by both water and proton during a 10 ns MD trajectory collected at 450 K. The migration of the water molecules from the tetrahedral cage (A) to the adjacent octahedral cage (B) forms a H_2O hydrogen-bonded bridge that connects the two types of cages through the triangular windows. This creates a path allowing the excess proton to jump from one cage to another. Such a proton transfer over long distances ensures a faster diffusivity and hence a higher conductivity as compared to ambient temperature.

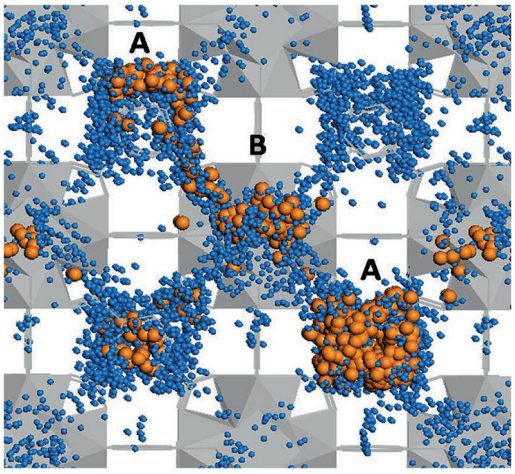

Figure 5. Illustration of the water (blue) -mediated pathway followed by the proton (orange) along the tetrahedral (A) and octahedral cages (B) of UiO-66(Zr)-$(CO_2H)_2$. aMS-EVB3-MD simulations performed at 450 K.

In summary, we evidenced that UiO-66(Zr)-$(CO_2H)_2$ shows a relatively high proton conductivity at 90 °C and 95% relative humidity which combined with a good water stability and a low cost and environmental friendly synthesis, makes this MOF among a few others as a promising candidate for further exploration in the field of solid-state proton-conducting technology. A microscopic picture of the proton transport in the best conducting MOFs has been missing. To address this challenging question, QENS experiments supported by MD simulations have proven to be valuable for probing distinctly the dynamics of both confined proton and water that has been only rarely achieved so far in proton conductors. This dual approach applied for the first time to MOFs reveals that the proton transfer over long distances is assisted by a hydrogen-bonded water network that forms a pathway that links the tetrahedral and the octahedral cages. This fundamental understanding might be of prime importance to tune the chemical and topological features of the MOFs for an optimization of their proton-conduction performances.

Experimental Section

MOF synthesis: The sample was prepared and activated according to a procedure described elsewhere.[17] For the QENS measurements, in order to reduce the scattering from the framework, a deuterated analogue UiO-66(Zr)-$(CO_2D)_2$ with formula $Zr_6O_4(OD)_4(O_2C\text{-}C_6D_2\text{-}CO_2\text{-}(CO_2D)_2)_6 \cdot x\,D_2O$ was prepared using synthetic conditions and activation from literature[17] (see the Supporting Information for the characterization data). The regular 1,2,4,5-benzenetetracarboxylic acid linker was replaced with the deuterium-enriched analogous molecule (D6; EI: 98% from Euriso-top), while the exchange of the hydrogen atoms of the μ_2-OH bridges was obtained by stirring the sample in boiling D_2O after activation.

Impedance measurements were performed on a broadband dielectric spectrometer, Novocontrol alpha analyzer over a frequency range from 1 Hz to 1 MHz with an applied ac voltage of 20 mV. The temperature T and relative humidity RH were controlled by an Espec Corp. SH-221 incubator in the ranges between 25–90 °C and 40–95% RH, respectively. Under these experimental conditions, the formation of anhydrides is prevented (see Figure S7). The samples were equilibrated for 24 h at given T and RH values, to ensure fixed water content. They were pressed under a pressure of 0.6 GPa to form pellets of the powder samples (2.02 mm thickness and 16 mm^2 surface). Pellets were sandwiched between two gold plates electrodes, allowing the two-probe method for electrical measurements. Resistivity was determined from the semicircles extrapolation in the Nyquist plots. Conductivity was calculated considering $\sigma = 1/R \times l/S$ where R is the impedance (Ω), σ is the conductivity ($S\,cm^{-1}$), l and S are the sample thickness (cm) and surface (cm^2), respectively.

QENS experiments: The measurements were performed at the Institut Laue-Langevin, using the time-of-flight spectrometer IN5. A high resolution of the order of 5 μeV (half-width at half-maximum, hwhm) was obtained with an incident neutron energy of 0.82 meV (10 Å). Low-energy spectra, where $\hbar\omega$ is the energy transfer, were measured at different scattering angles. The wave-vector transfer, Q, is related to the scattering angle, the presence of strong Bragg peaks

restricting the number of spectra to the Q range 0.2–0.96 Å^{-1}. During a QENS experiment, motions which occur in space and in time are measured in $Q-\omega$ space through Fourier transform. The observed intensities are thus presented here in terms of the scattering function, $S(Q,\omega)$, also called dynamical structure factor. Information on translational and rotational motions can be obtained by analyzing the quasi-elastic broadenings at small energy transfers, as a function of wave-vector transfer. Regarding the data analysis, the weighted profile factor R_{wp} is defined as shown in Equation (1),

$$R_{wp} = \left(\sum_i w_i [y_i(\text{obs}) - y_i(\text{calc})]^2 \Big/ \sum_i w_i [y_i(\text{obs})]^2 \right)^{1/2} \quad (1)$$

where y_i(obs) and y_i(calc) denote the experimental and calculated values, and the weight is $w_i = 1/y_i(\text{obs})$. Two samples were prepared after desorption at 373 K: the first one fully hydrated (120 H_2O per unit cell) and the second one desorbed, the weight of the MOF being identical for the two samples. The scattering from the empty MOF was subtracted from the spectra recorded with the loaded sample, after normalization and corrections with standard programs.

aMS-EVB3 MD Simulations: These calculations were performed at four different temperatures ($T = 300$, 350, 400, and 450 K) using the DL-POLY-2[41] software with a simulation box containing one cubic unit cell of UiO-66(Zr)-$(CO_2H)_2$ containing H_2O molecules. The initial distribution of water molecules as preliminary obtained by Grand Canonical Monte Carlo simulations performed at $p/p^0 = 1$ (80 H_2O per unit cell) while the excess proton was randomly added to one H_2O molecule to form the initial H_3O^+ ion. The UiO66-$(CO_2H)_2$ was treated by using our previously reported flexible force field[17] while the aqueous proton was treated by the aMS-EVB3 model and the water by the aSPC/Fw force field.[16,33] The MOF/water and MOF/hydronium interactions were obtained using the Lorentz–Berthelot mixing rules. This approach is capable of mimicking the proton hopping between water molecules at infinite proton dilution.[42] The position of the center of the excess charge (CEC) is explicitly given by the vector $\mathbf{r}_{CEC} = \sum_i c_i^2 \mathbf{r}_i$, where c_i^2 is the probability and $\mathbf{r}_i$ is the position of the center of charge in the hydronium in ith EVB state.[42,43] This protonated system was equilibrated for at least 2 ns in the NVT ensemble using Nosé–Hoover thermostat with a relaxation time of 1 ps. After equilibration, 5 trajectories of 2 ns and a few trajectories of 20 ns were collected for each temperature in the NVE ensemble.

Acknowledgements

We thank the Institut Laue-Langevin (Grenoble, France) for the neutron beam time. F.P. acknowledges support from the National Science Foundation (award number DMR-1305101) and the U.S. Department of Energy, Office of Science (award number DE-FG02-13ER16387). The research leading to the synthesis of the samples (ILV) has received funding from the European Community Seventh Framework Program (FP7/2007-2013) under grant agreement number 608490 (project M^4CO_2). G.M. thanks Institut Universitaire de France for support. A. Vimont and P. Bazin are warmly thanked for the infrared characterization.

Keywords: metal–organic frameworks · microscopic mechanism · molecular dynamics · proton conduction · quasi-elastic neutron scattering

How to cite: *Angew. Chem. Int. Ed.* **2016**, *55*, 3919–3924
Angew. Chem. **2016**, *128*, 3987–3992

[1] A. Kraytsberg, Y. Ein Eli, *Energy Fuels* **2014**, *28*, 7303.
[2] A. Mallick, T. Kundu, R. Banerjee, *Chem. Commun.* **2012**, *48*, 8829.
[3] T. Yamada, K. Otsubo, R. Makiura, H. Kitagawa, *Chem. Soc. Rev.* **2013**, *42*, 6655.
[4] M. Yoon, K. Suh, S. Natarajan, K. Kim, *Angew. Chem. Int. Ed.* **2013**, *52*, 2688; *Angew. Chem.* **2013**, *125*, 2752.
[5] P. Ramaswamy, N. E. Wong, G. K. H. Shimizu, *Chem. Soc. Rev.* **2014**, *43*, 5913.
[6] S. Horike, D. Umeyama, S. Kitagawa, *Acc. Chem. Res.* **2013**, *46*, 2376.
[7] W. J. Phang, H. Jo, W. R. Lee, J. H. Song, K. Yoo, B. S. Kim, C. S. Hong, *Angew. Chem. Int. Ed.* **2015**, *54*, 5142; *Angew. Chem.* **2015**, *127*, 5231.
[8] J. M. Taylor, K. W. Dawson, G. K. H. Shimitzu, *J. Am. Chem. Soc.* **2013**, *135*, 1193.
[9] V. G. Ponomareva, K. A. Kovalenko, A. P. Chupakhin, D. N. Dybtsev, E. S. Shutova, V. P. Fedin, *J. Am. Chem. Soc.* **2012**, *134*, 15640.
[10] M. Sadakiyo, H. Okawa, A. Shigematsu, M. Ohba, T. Yamada, H. Kitagawa, *J. Am. Chem. Soc.* **2012**, *134*, 5472.
[11] S. Bureekaew, S. Horike, M. Higuchi, M. Mizuno, T. Kawamura, D. Tanaka, N. Yanai, S. Kitagawa, *Nat. Mater.* **2009**, *8*, 831.
[12] S. Horike, W. Chen, T. Itakura, M. Inukai, D. Umeyama, H. Asakurae, S. Kitagawa, *Chem. Commun.* **2014**, *50*, 10241.
[13] P. Ramaswamy, N. E. Wong, B. S. Gelfand, G. K. H. Shimizu, *J. Am. Chem. Soc.* **2015**, *137*, 7640.
[14] K. D. Kreuer, A. Rabenau, W. Weppner, *Angew. Chem. Int. Ed. Engl.* **1982**, *21*, 208; *Angew. Chem.* **1982**, *94*, 224.
[15] C. J. D. Grotthuss, *Ann. Chim.* **1806**, *58*, 54.
[16] F. Paesani, *J. Phys. Chem. C* **2013**, *117*, 19508.
[17] Q. Yang, et al., *Angew. Chem. Int. Ed.* **2013**, *52*, 10316; *Angew. Chem.* **2013**, *125*, 10506.
[18] F. Ragon, et al., *J. Mater. Chem. A* **2015**, 3, 3294.
[19] P. Colomban in *Proton Conductors: Solids, Membranes, and Gels-Materials and Devices*, Cambridge University Press, Cambridge, **1992**.
[20] H. Jobic, D. N. Theodorou, *Microporous Mesoporous Mater.* **2007**, *102*, 21.
[21] F. Salles, H. Jobic, G. Maurin, M. M. Koza, P. L. Llewellyn, T. Devic, C. Serre, G. Férey, *Phys. Rev. Lett.* **2008**, *100*, 245901.
[22] E. Pantatosaki, H. Jobic, D. I. Kolokolov, S. Karmakar, R. Biniwale, G. K. Papadopoulos, *J. Chem. Phys.* **2013**, *138*, 034706.
[23] H. Jobic, J. Karger, M. Bee, *Phys. Rev. Lett.* **1999**, *82*, 4260.
[24] M. Karlsson, *Phys. Chem. Chem. Phys.* **2015**, *17*, 26.
[25] J. C. Lassègues, D. Cavagnat, *Phys. B* **1992**, *180–181*, 645.
[26] Q. Berrod, S. Lyonnard, A. Guillermo, J. Ollivier, B. Frick, G. Gébel, *EPJ Web Conf.* **2015**, *83*, 02002.
[27] A. Desmedt, F. Stallmach, R. E. Lechner, D. Cavagnat, J. C. Lassègues, F. Guillaume, J. Grondin, M. A. Gonzalez, *J. Chem. Phys.* **2004**, *121*, 11916.
[28] A. Desmedt, R. E. Lechner, J. C. Lassègues, F. Guillaume, D. Cavagnat, J. Grondin, *Solid State Ionics* **2013**, *252*, 19.
[29] L. Bedouret, P. Judeinstein, J. Ollivier, J. Combet, A. Desmedt, *J. Phys. Chem. B* **2014**, *118*, 13357.
[30] T. Yamada, H. Kitagawa, M. Tyagi, V. G. Sakai, O. Yamamuro, *Phys. Chem. Chem. Phys.* **2014**, *16*, 17295.
[31] K. Krynicki, C. D. Green, D. W. Sawyer, *Faraday Discuss. Chem. Soc.* **1978**, 66, 199.
[32] N. K. Roberts, L. N. Helen, *J. Chem. Soc. Faraday Trans.* **1974**, *70*, 253–262.
[33] K. Park, W. Lin, F. Paesani, *J. Phys. Chem. B* **2012**, *116*, 343–352.
[34] Y. Wu, H. Chen, F. Wang, F. Paesani, G. A. Voth, *J. Phys. Chem. B* **2008**, *112*, 467–482.
[35] J. M. J. Swanson, C. M. Maupin, H. Chen, M. K. Petersen, J. Xu, Y. Wu, G. A. Voth, *J. Phys. Chem. B* **2007**, *111*, 4300.

[36] R. Semino, D. Laria, *J. Chem. Phys.* **2012**, *136*, 194503.
[37] A. Chandra, M. E. Tuckerman, D. Marx, *Phys. Rev. Lett.* **2007**, *99*, 145901.
[38] T. C. Berkelbach, H. S. Lee, M. E. Tuckerman, *Phys. Rev. Lett.* **2009**, *103*, 238302.
[39] M. Eigen, *Angew. Chem. Int. Ed. Engl.* **1964**, *3*, 1; *Angew. Chem.* **1963**, *75*, 489.
[40] W. L. Jorgensen, C. Jenson, *J. Comput. Chem.* **1998**, *19*, 1179.
[41] DL-POY-2.0: A General-Purpose Parallel Molecular Dynamics Simulations Package. W. Smith, T. R. Forester, *J. Mol. Graphics* **1996**, *14*, 136.
[42] U. W. Schmitt, G. A. Voth, *J. Chem. Phys.* **1999**, *111*, 9361.
[43] T. J. Day, A. V. Soudackov, M. Cuma, U. W. Schmitt, G. A. Voth, *J. Chem. Phys.* **2002**, *117*, 5839.

Received: November 23, 2015
Published online: February 17, 2016

